Radiation Hard Silicon Photonics Mach-Zehnder Modulator for HEP applications: all-Synopsys Sentaurus™ Pre-Irradiation Simulation

Simone Cammarata, *University of Pisa, CERN (Summer Student)*
Jan Troska, *CERN (1st Supervisor)*
Francois Vasey, *CERN (2nd Supervisor)*

***Abstract*— *Silicon Photonics* may well provide the opportunity for new levels of integration between detectors and their readout electronics. This technology is thus being evaluated at CERN in order to assess its suitability for use in particle physics experiments.**

In order to check the agreement with measurements and the validity of previous device simulations, a pure *Synopsys Sentaurus™* simulation of an un-irradiated Mach-Zehnder silicon modulator has been carried out during the Summer Student project.

***Index Terms*—Silicon Photonics, Mach-Zehnder modulator, electro-optic simulation, Synopsys Sentaurus™, electro-optic measurement, HEP.**

I. Introduction

Silicon photonic (SiPh) components can enable new design paths for future optical read-out systems designed for environments with high radiation levels. They potentially offer:

- High data rates (chance of wavelength multiplexing)
- Reduced fibre count in detector
- Possibility for integration or hybridization with driving electronics and silicon particle sensors
- Increased chip functionality, decreased assembly costs harnessing advanced and mature silicon technologies
- Radiation hardness similar to silicon particle detectors (with remote laser source)
- Positioning of components closer to interaction point, elimination of copper wiring

First results from radiation tests indicate that SiPh Mach-Zehnder modulators (MZMs) are almost insensitive to neutron radiation. However, their performance degrades strongly when exposed to x-rays [2]. SiPh MZMs with varied process parameters have been designed during previous years by EP-ESE-BE group at CERN to develop custom devices with improved resistance against ionizing radiation.

To get a better idea of the influence of radiation on the device performance and to find design strategies to improve the radiation hardness device simulations were performed.

The goal of the Summer Student project was the realization of a pre-irradiation simulation of a MZM including the structure generation, the device simulation and the optical mode extraction using solely Synopsis Sentaurus™ (TCAD) tools. This work could be useful to check the validity of previous results (both measured and simulated) and to discover the potential applicability of some Synopsys Sentaurus™ software packages to our purposes.

All the work done doesn't include any kind of radiation damage modeling or transient analysis for damage effects investigation; who is interested can find further information on these topics here [1].

II. Silicon Mach-Zehnder Modulator

The Mach-Zehnder modulator (MZM) is one of the most common photonic modulator types fabricated in integrated opto-electronics today. Its main purpose is to convert an elecrical data stream into an optical one. It is based on the Mach-Zehnder Interferometer (MZI) structure and, as with every interferometer, the optical output power is modulated by means of interfering light beams.

As shown in Fig. 1, the incoming light is split in two beams, each one experiencing a different optical path length. Depending on the path length difference, both light beams accumulate different phases with respect to each other until the point where they recombine.

This phase difference can be exploited to produce either constructive or destructive interference[1] at the combiner output. In an integrated MZM this interference behaviour is applied to data transmission (converting a 0/1 electrical-level into a 0/1 optical-level).

In order to achieve this phase lag between the two beams we can embed a voltage-controlled phase shifter in one or both[2] the waveguide arms. In this way an electrical signal can induce the desired modulation of the optical power flowing out of the MZM.

Phase shifters perform a local change to the material's refractive index $n \rightarrow (n \pm \Delta n(x,y,z)) \equiv (n \pm \Delta n(x,y))$ that also affects the *effective* index $n_{\text{eff}} \rightarrow (n_{\text{eff}} \pm \Delta n_{\text{eff}})$ of the guided mode in MZM's waveguides. The resulting phase difference between the two beams after the light has travelled through the phase shifters can be expressed as [3]

$$\Delta\phi = \frac{2\pi \Delta n_{\text{eff}} L}{\lambda} \tag{1}$$

[1]Constructive interference occurs when the two beams are in-phase, i.e. when the phase difference between the two arms obeys $\Delta\phi = 2\pi m$ with m being an integer. Destructive interference can be observed for $\Delta\phi = \pi m$ when m is an odd integer.

[2]One can think about some *push-pull* driving techniques to halven the requirements for a single phase shifer.

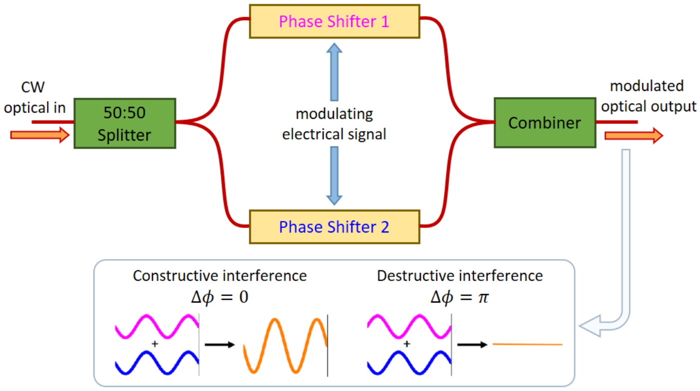

Fig. 1: Principle of an MZM showing the conditions for the phase shift that lead to constructive and destructive interference at its output. In red the waveguides are drawn.

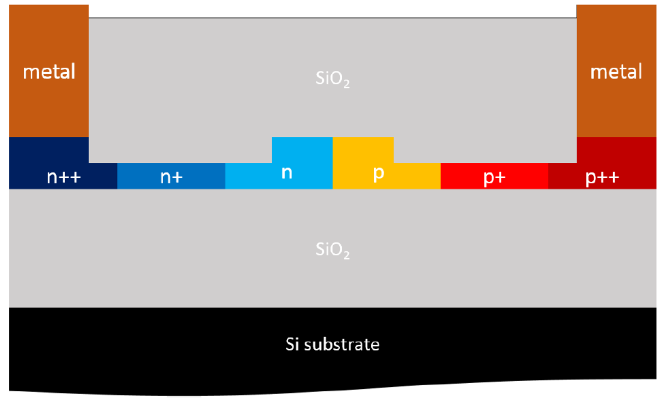

Fig. 2: Qualitative schematic of a depletion mode phase shifter with a lateral pn-junction.

where L is the waveguide physical length and λ is the operating wavelength (in this case 1.55µm).

The changes in the effective refractive index Δn_{eff} are determined by the overlap integral between the optical mode and the region where the refractive index has changed [3]

$$\Delta n_{\text{eff}} = \iiint_{-\infty}^{+\infty} \frac{\Delta n(x,y,z)|\vec{E}(x,y,z)|^2}{|\vec{E}(x,y,z)|^2}\,dx\,dy\,dz \tag{2}$$

with $\vec{E}$ being the electric field of the optical mode, (x, y) the transverse coordinates and z the propagation direction.

Refractive index perturbations and electric field modulus z-dependence could be neglected because we can consider the waveguide uniform along the longitudinal direction. Hence, previous equation becomes:

$$\Delta n_{\text{eff}} = \iint_{-\infty}^{+\infty} \frac{\Delta n(x,y)|\vec{E}(x,y)|^2}{|\vec{E}(x,y)|^2}\,dx\,dy \tag{3}$$

A. *Plasma Dispersion effect in Silicon*

Even though silicon doesn't exhibit any kind of linear electro-optic effect[3], we can induce local refractive index changes in the material by *Plasma Dispersion* effect.

This is a process in which changes in absorption of photons (that are directly coupled to changes in refractive index by Kramers-Kronig relations) are induced through changes in charge carrier concentration.

A simple physical explanation is that, even if silicon is transparent to telecommunications wavelengths[4], some *intra-band* absorption occur among charge carriers in the same band. Varying carrier concentration in a region of the semiconductor leads to a change in the amount of this intraband absorptions and then to a modification of the refractive index of that zone.

Soref and Bennett, in their pioneering work [4], evaluated an empirical formula to get the complex refractive index (CRI) variation $\Delta\tilde{n} = \Delta n + i\Delta\alpha$ as a function of free carrier concentrations $N_e \equiv N_e(x,y,z)$ and $N_h \equiv N_h(x,y,z)$ (for $\lambda = 1.55$µm)

$$\begin{aligned}\Delta n(x,y,z) &= -8.8\cdot 10^{-22}N_e + 6.0\cdot 10^{-18}(N_h)^{0.8}\\ \Delta\alpha(x,y,z) &= 8.5\cdot 10^{-18}N_e + 6.0\cdot 10^{-18}N_h\end{aligned} \tag{4}$$

B. *Phase Shifting Depletion-mode Rib waveguide*

The simplest way to achieve a voltage-controlled carrier movement inside an SOI rib waveguide is to incorporate a pn junction. There are several ways to implement it [5]. In this work we focus on *depletion-mode* MZMs due to their suitability for HEP applications [3] because of the improved radiation resistance and the low power consumption.

The pn junction is lateral (see Fig. 2) and reverse-biased. By changing the bias voltage we can change the width of the depletion region, so the amount of free carriers that overlaps with the propagating optical mode is controlled.

Different bias voltages V_{bias} lead to different effective indexes $\Delta n_{\text{eff}}(V_{\text{bias}})$ resulting in different overall phase shifts $\Delta\phi(V_{\text{bias}})$ at the end of the waveguide.

III. Simulating Phase Shifting Rib waveguide

To ensure the functionality and optimise the efficiency of a MZM, the phase shift vs. voltage characteristic was simulated. *Steady-state* electro-optical simulations were performed to predict the performance of a potential device design.

The goal is to extract the phase shift for a given modulator length[5]. The phase shift in respect to the $V_{\text{bias}} = 0\,\text{V}$ case is calculated for different reverse bias voltages using already computed overlap integrals $\Delta n_{\text{eff}}(V_{\text{bias}})$

$$\begin{aligned}\Delta\Phi(V_{\text{bias}}) &= \Delta\phi(V_{\text{bias}}) - \Delta\phi(0\,\text{V})\\ &= \frac{2\pi L}{\lambda}\Big(\Delta n_{\text{eff}}(V_{\text{bias}}) - \Delta n_{\text{eff}}(0\,\text{V})\Big)\end{aligned} \tag{5}$$

[3]There would be some in a strained waveguide, but this falls outside the scope of this report.

[4]No conduction-to-valence band absorption is energetically possible.

[5]Intuitively, the longer the modulator the larger the phase shift we get because there's more interaction between photons and charge carriers. In other words, the optical mode sees for a longer distance the refractive index change so it can accumulate much more phase lag at the end of the waveguide.

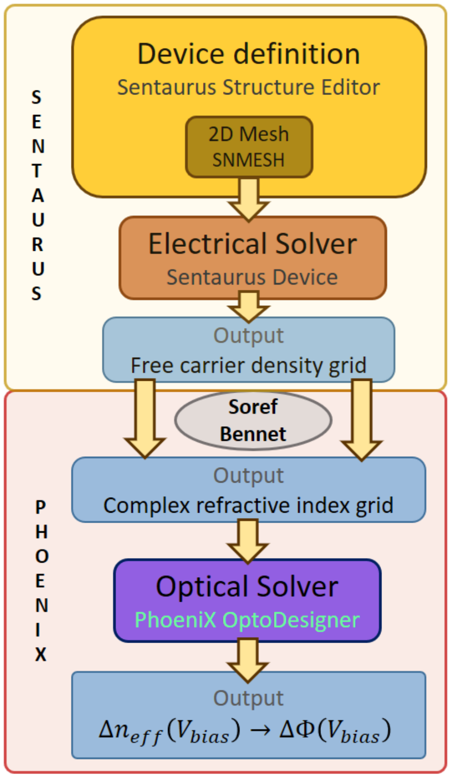

Fig. 3: Flow chart showing how Sentaurus$^{\mathrm{TM}}$ and PhoeniX$^{\mathrm{TM}}$ tools are used to model DC-performance of an un-irradiated MZM.

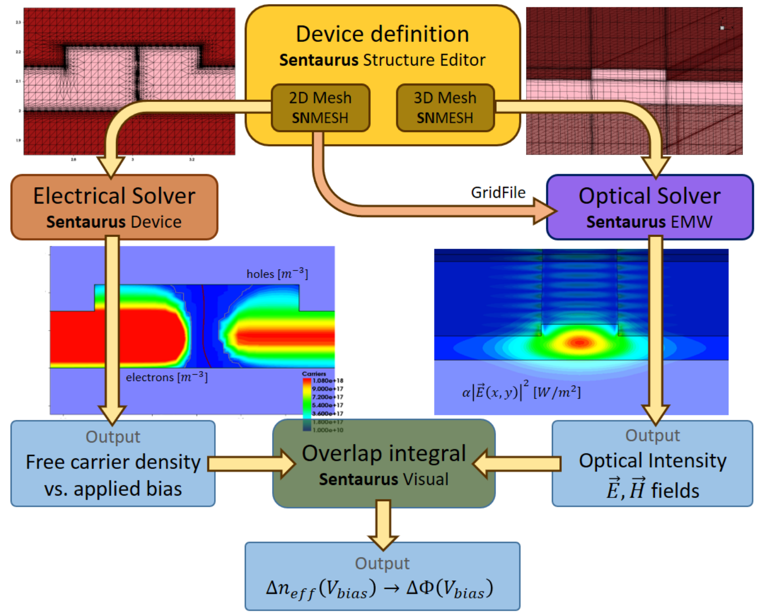

Fig. 4: Flow chart for an all-Sentaurus$^{\mathrm{TM}}$ simulation of an un-irradiated MZM.

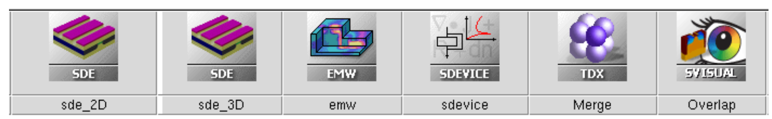

Fig. 5: Tool flow in all-Sentuarus$^{\mathrm{TM}}$ simulation.

This gives the phase shift expressed in rad. To eliminate the length dependence and to compare modulators with different lengths the phase shift is expressed in $\frac{\pi}{\mathrm{mm}}$

$$\begin{aligned}\Delta\Phi_{\frac{\pi}{\mathrm{mm}}}(V_{\mathrm{bias}}) &= \frac{\Delta\Phi(V_{\mathrm{bias}})}{L} \\ &= \frac{2}{\lambda[\mathrm{mm}]}\Big(\Delta n_{\mathrm{eff}}(V_{\mathrm{bias}}) - \Delta n_{\mathrm{eff}}(0\,\mathrm{V})\Big)\end{aligned} \tag{6}$$

Our main goal is then to develop a numerical simulation in order to evaluate this phase shifts $\Delta\Phi_{\frac{\pi}{\mathrm{mm}}}(V_{\mathrm{bias}})$ for some custom designed devices. They are basically four:

- Shallow etch, nominal doping
- Deep etch, nominal doping
- Shallow etch, doubled doping
- Deep etch, doubled doping

where *shallow/deep* etch refers to the slab thickness of the waveguide[6] and *doubled* doping means that doping concentrations in the rib region are set to be two times the nominal values.

A. Previous simulations

As shown in Fig. 3, a cross-sectional 2D phase shifter model (for each kind of device) is defined in Synopsys Sentaurus$^{\mathrm{TM}}$ TCAD [11] and the embedded electrical solver is used to simulate the electrical properties of the pn-junctions under bias to determine electron and hole densities in the silicon layer.

The carrier densities are extracted from Sentaurus$^{\mathrm{TM}}$ Device and converted with the Soref-Benett formulas (4) to a uniform grid of complex refractive indices. The resulting changes in $\Delta n_{\mathrm{eff}}(V_{\mathrm{bias}})$ are then computed with a finite-difference mode solver in the OptoDesigner$^{\mathrm{TM}}$ software from PhoeniX$^{\mathrm{TM}}$ [12]. The phase shift $\Delta\Phi(V_{\mathrm{bias}})$ resulting from a voltage change is finally calculated with equation (6).

Despite the straightforward simulation flow, this kind of approach leads to the use of two different software packages. This means two separate license to buy and some "bridge-like" solution to make an output file from one software understandable by the other one.

These reasons led to the implementation of a pure Synopsys Sentaurus$^{\mathrm{TM}}$ workflow, using its integrated finite-difference electromagnetic solver (EMW) for the optical mode extraction.

IV. All-Synopys Sentaurus$^{\mathrm{TM}}$ Electro-optic Simulation

The simulation that we did calculates independently the fundamental optical mode of the waveguide and the free carrier densities, then it computes the overlap integral (3) for each device type and bias voltage (that will be one of these values $[0\,\mathrm{V},\ 1\,\mathrm{V},\ 2\,\mathrm{V},\ 3\,\mathrm{V}]$[7]).

Software packages used from Synopsys$^{\mathrm{TM}}$ toolkit are:

[6]The shallower the etch the thicker the slab and the deeper the etch the thinner the slab. See next figures for further clarifications.

[7]Attention! They are all intended as *reverse* bias voltages.

- *Sentaurus Structure Editor* (SDE): used to define the structure of the SOI waveguide. Geometry, materials and doping profiles are defined in a script written using built-in SDE commands.
- *Sentaurus Mesh Generator* (SNMESH): usually embedded in SDE scripts, is used to create the discretized mesh files needed by other Sentaurus tools to make their computations. SNMESH creates two different type of mesh files: the *tensor* mesh, used for electromagnetic simulations, and the *mixed-element* mesh, suitable for the electrical calculations.
- *Sentaurus Electromagnetic Wave Solver* (EMW): deployed for finding the optical mode distribution in the cross section of the waveguide. It is based on a FDTD method to solve Maxwell's equations.
- *Sentaurus Device* (SDEV): numerically solves equations governing carrier transport (Poisson, carrier-continuity, etc.). It takes as input the 2D mesh generated by SDE and then fills up a grid output file with free carriers concentrations for each bias voltage. This part of the work it is almost completely inherited from past simulations; details on implemented physical models can be found in [6] and [9].
- *Sentaurus Data Explorer* (TDX) and Sentaurus Visual (SVIS): are used to access data from grid files (`.tdr` extension). It is possible to create custom datasets and visualize them.

A flowchart of the entire process is shown in Fig. 4 and a sketch of the tool flow is in Fig. 5.

A. Waveguide Design

In order to have a single-mode rib waveguide some constraints within the aspect ratio must be complied. These conditions lead to the structure displayed in Fig. 6, where all the geometrical parameters shown are chosen to allow only fundamental modes (TE and TM) to propagate into the waveguide, see [7] for further info regarding single-mode condition (SMC).

The waveguide design is divided in two branches: one that creates a 2D structure for SDEV and the other that builds a 3D mesh for EMW.

- `sde_2D`: the output of this tool is basically the one in Fig. 6. There are two important things to notice:
  - SiO_2 regions close to the silicon-oxide interface was defined as *OxideAsSemiconductor* in order to allow dieletric areas to have nonzero conductivity. This feature would become very useful once radiation damage modeling is included in the simulation[8].
  - Because the discretized mesh should be denser in sensitive regions of the device, some additional refinements are implemented on the silicon-oxide interface and in areas where there is an high gradient of doping concentrations. The resulting 2D *mixed-element* mesh is made only of triangles, see Fig. 7.

[8]Movements of trapped charges (generated by ionizing radiation in the oxide layers) could be effectivily simulated.

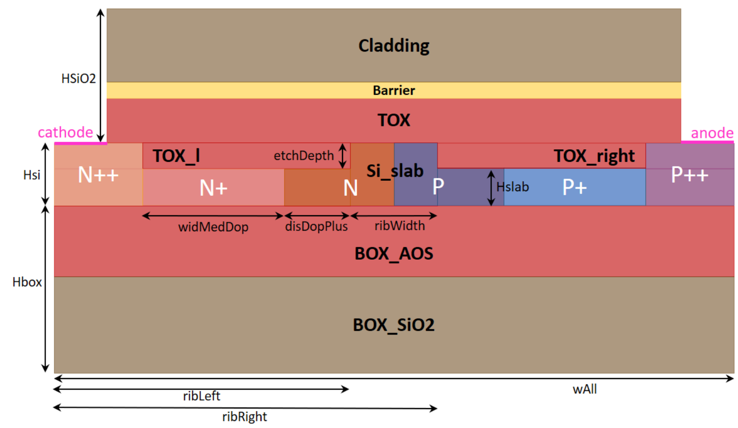

Fig. 6: Schematic of the simulated structure cross section. Except the easily recognisable silicon layer, the other materials are: OxideAsSemiconductor (red), SiO_2 (brown), Si_3N_4 (yellow).

- `sde_3D`: this structure is generated extruding the previous 2D cross section by a length defined by the parameter `deviceLength` in the command file. It is worth to highlight some differences with respect to the other mesh:
  - It seemed that it is impossible to run an optical simulation with the *OxideAsSemiconductor* material: the software engine gives an error concerning a non-existing reference to its CRI model. Therefore, all the "oxide-like" material were set to SiO_2 in the 3D mesh[9].
  - This mesh is a *tensor* grid mesh fully made of rectangles, that should be as uniform as possible throughout the structure because the accuracy of the FDTD method critically depends on cell size and mesh uniformity[10] [8]. In our case a little refinement (see Fig. 7) on silicon-oxide interface is implemented.
    To control the tensor mesh generation (for EMW purposes) there is a command to specify the number (`npw`) of mesh vertexes per wavelength to be placed inside a given material or region. Usually there should be al least 10 points per wavelength to get reasonable results. On the other hand, choosing too many points per wavelength, there is the risk to get a non-convergent simulation.

B. Electromagnetic Wave Solver

The solver starts by placing a truncated-plane wave source close to the open end of the waveguide. The excitation plane is defined to be parallel and comparable in size to the rib

[9]It would not even have been a problem because additional properties of *OxideAsSemiconductor* that make it different from SiO_2 can come out only in the simulation of an irradiated sample.

[10]Numeric dispersion of FDTD method increases when the cells have large aspect ratios or abrupt grading.

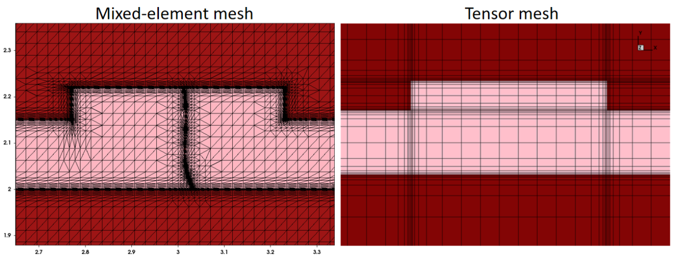

Fig. 7: Grid-element and tensor meshes.

region. It is used to excite propagation of a TE mode (all fields components $= 0$ expect E_x, E_y, $H_z \neq 0$) with a wavelength $\lambda = 1.55$µm.

Attention! The excitation plane has to stay a few grid points away from the structure facet. For example, using a too low `npw` there is the possibility to come up with something like: "Error: impossible to apply TFSF (Total Field Scattered Field) method to anisotropic dieletric media". This is due to the lack of grid points between excitation plane and material interface, so the engine finds a non-isotropic enviroment where it can not apply its numerical method. Possible solutions could be: increase the distance plane-waveguide or increase `npw`.

We only concern about TE mode because we know that in real applications, i.e. in our fabricated test chip, there will be only that mode propagating. This is due to the fact that we are coupling light in our chips by means of grating couplers that are polarization-sensitive to only TE mode, and therefore they strongly attenuate TM polarization state.

The simulation converges when, for each field component, the difference in amplitude of the fields between detection periods divided by the maximum field value in the detection window[11] is smaller than the parameter `tolerance`. This value has a big influence on the simulation time (it should be around 10^{-2}, or at most 10^{-3}).

EMW can generate 3 types of output files:

- 3D grid file (from `Save{}` section): all electromagnetic field quantities and power fluxes are stored for each point of the 3D mesh.
- 2D grid file on tensor mesh (from `Extractor{}` section): is generated extracting a plane (at z coordinate specified in the command file) from the 3D grid file.
- 2D grid file on mixed-element mesh (from `Extractor {}` section): is generated extracting a tensor-grid plane at the desired z coordinate from 3D grid and then interpolating all fields values onto the specified 2D mesh.

Attention! Normally, inside an `Extractor{}` section you specify, by means of `BoxCorner` commands, the plane[12] or cuboid where the EMW output should be extracted.

[11] Specified in the `Detector{}` section of the command file.

[12] Taking z coordinate fixed, i.e. `BoxCorner1 = (x1, y1, z)` and `BoxCorner2 = (x2, y2, z)`.

	Measured $\Delta\Phi_{\frac{\pi}{mm}}(V_{bias})$	
V_{bias}	Shallow etch	Deep etch
$0\,V$	0.000	0.000
$1\,V$	0.099 ± 0.012	0.063 ± 0.012
$2\,V$	0.177 ± 0.020	0.125 ± 0.016
$3\,V$	0.255 ± 0.024	0.177 ± 0.016

Table I: Measured phase shifts, taken from [3].

Extracting a 2D tensor grid file results in the plane at the chosen z-coordinate.
Instead, making a z-cut in the 3D simulated structure to interpolate the extracted tensor plane on a 2D mixed-element mesh it will not work.
This is because, specifying the 2D mesh file with the `GridFile` option, the `BoxCorner` commands will automatically refer to the loaded mesh and not anymore to the 3D EMW structure. Indeed, extracting the final plane of the structure, e.g. at $z = 10.0\,\mu\text{m}$, we will end up with the electromagnetic fields at the beginning of the waveguide, because in the 2D mesh there is only the $z = 0.0\,\mu\text{m}$ plane!
In Fig. 8 there are some explanatory plots.

The problem is that we want to extract an optical mode far away from the excitation plane, because non-ideal excitations can locally[13] excite higher order modes, that can perturb our cross sectional optical intensity distribution until they fail to be guided [10].
The best solution we have found so far is to place the excitation window at the end of the 3D mesh (with wave's $\vec{k}$ vector pointing towards the $z = 0.0\,\mu\text{m}$ facet). In this way, the plot extracted in the `Extractor{}` section is related to the end of the propagation of the optical wave.

V. Handling Results and Comparison with Previous Simulations and Measurements

According to theory that we have derived so far, we need to calculate the electric field modulus $|\vec{E}|^2$ on the waveguide cross section to apply equations (1) and (3). Since we should[14] have a TE mode ($E_z = 0$) this is equal to the transverse electric field $|\vec{E}|^2 = |\vec{E}_T|^2 = |E_x|^2 + |E_y|^2$. There are two ways to compute $|\vec{E}_T|^2$:

- Use TDX tool to evaluate it directly from simulated electromagnetic quantities and put it in a new dataset.
- Use an already existing EMW dataset called `OpticalGeneration` that should be proportional to it, according to [9].

Unfortunately, in both cases, plotting $|\vec{E}_T|^2$ on the 3D tensor mesh we can notice an unexpected periodicity of its modulus along the direction of propagation (see Fig. 9) that is not predicted by theory[15].
In Tab. III and IV phase shift values evaluated using $|\vec{E}_T|^2$ from different z-cuts are shown. As expected, phase shift

[13] Usually in the first hundreds of nm of propagation.

[14] Even though we could have unwanted numerical fluctuations.

[15] The whole report relies on the fact that the optical mode is constant along the structure.

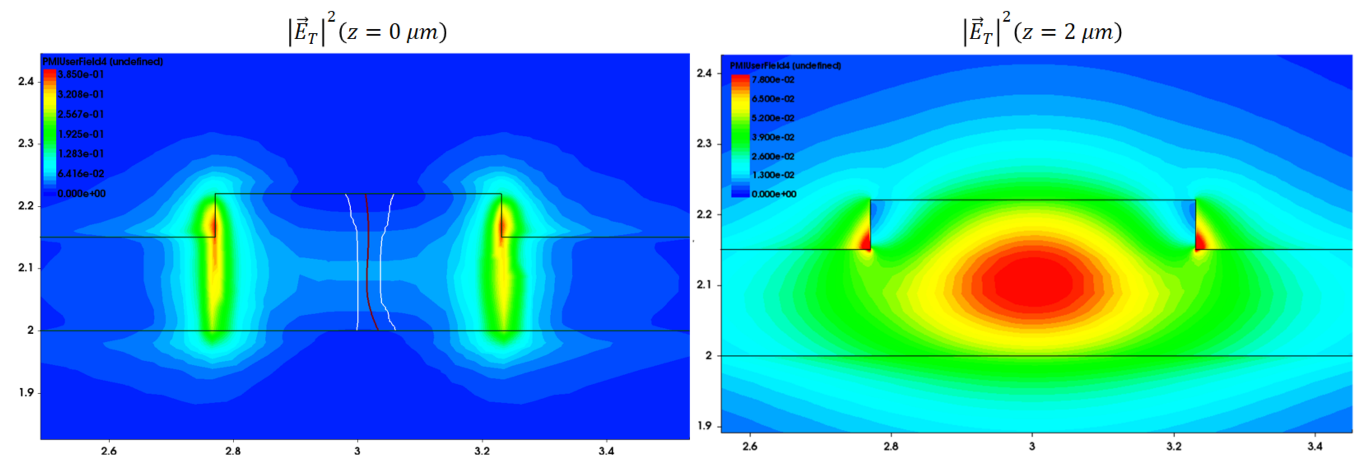

Fig. 8: Simulated modulus squared of the transverse electric field along the waveguide with plane excitation placed at $z = 0.0\,\mu\text{m}$. On the left there is the initial unexpected field distribution and on the right, after $2.0\,\mu\text{m}$ of propagation, we can appreciate a reasonable fundamental mode.

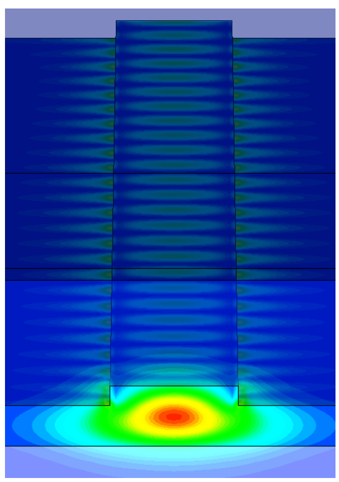

Fig. 9: $|\vec{E}_T|^2$ plot of a $10.0\,\mu\text{m}$-long device. Along direction of propagation there are amplitude fluctuations.

values are "length-dependent" and greater values corresponds to planes where the electric field modulus is bigger.

A comparison between this data and measured ones shows that we have a good agreement for the biggest phase shift values extracted from the simulation, see Tab. I and Tab. II.

This means that, even though there is not a clear understanding of the periodicity in the simulation results, we could still compare the measurement data to the simulation when selecting a z-cut close to one of the maxima of the $|\vec{E}_T|^2$ distribution. Certainly, this is not a final result and this behaviour needs to be further investigated in future work.

VI. Conclusion and Further Developments

We have presented an all-Synopsys Sentaurus™ simulation of an unirradiated MZM showing the toolflow and the main issues that we solved.

Further development needs to be carried out to better understand the unexpected periodicity of the optical mode intensity distribution along the propagation direction.

Due to the presented results further steps could be:

- Building a 3D mesh also for the electrical simulation. In this way, there would be the possibility to arbitrarily select the plane to use for optical data interpolation on 2D mixed-element mesh. This kind of approach could be particularly time consuming because two 3D numerical computations are involved.
- Coming back to previous simulation (Fig. 3) concept but using only Synopsys Sentaurus™ software packages. There would be the need to reverse the order of EMW and SDEV with respect to the current toolflow. SDEV has to be used to calculate a dataset for CRI, exploiting a custom model interface (CRIMI) that implements Soref Bennett formulas. Hence, EMW should be configured to read SDEV's output file and activate the spatially-dependent CRI feature.

For all these future tasks agreement with meausured data and dependence on simulation parameters have to be checked in order to get a reliable model to start studying radiation effects.

Acknowledgment

The author would like to thank A. Kraxner, C. Scarcella, S. Seif El Nasr-Storey and all the EP-ESE-BE group for their support during the work.

References

[1] S. Seif El Nasr-Storey, *Effect of Radiation on a Mach-Zehnder Interferometer Silicon Modulator for HL-LHC Data Transmission Applications*, *IEEE Transactions on Nuclear Science*, vol. 62, 2015.

[2] S. Seif El Nasr-Storey, *Modeling TID effects in Mach-Zehnder Interferometer Silicon Modulator for HL-LHC Data Transmission Applications*, *IEEE Transactions on Nuclear Science*, vol. 62, 2015.

[3] M. Zeiler, *Radiation-hard silicon photonics for future high energy physics experiments*, PhD Thesis, 2017.

[4] R. Soref, B. Bennett, *Electrooptical effects in silicon*, *IEEE Journal of Quantum Electronics*, vol. 23, pp. 123-129, 1987.

	$\Delta\Phi_{\frac{\pi}{mm}}(V_{bias})$			
	Shallow etch		Deep etch	
V_{bias}	Measured	Simulated ($z = 2.00\,\mu m$)	Measured	Simulated ($z = 0.00\,\mu m$)
0 V	0.000	0.000	0.000	0.000
1 V	0.099 ± 0.012	0.106	0.063 ± 0.012	0.068
2 V	0.177 ± 0.020	0.185	0.125 ± 0.016	0.120
3 V	0.255 ± 0.024	0.257	0.177 ± 0.016	0.168

Table II: Comparison between measured (from [3]) and simulated phase shifts of a $10.0\,\mu m$-long device (normal doping). Simulated ones are selected from Tab. III and Tab. IV taking the maximum values.

	$\Delta\Phi_{\frac{\pi}{mm}}(V_{bias})$								
V_{bias}	$z = 0.00\,\mu m$	$z = 1.00\,\mu m$	$z = 2.00\,\mu m$	$z = 3.00\,\mu m$	$z = 4.00\,\mu m$	$z = 5.00\,\mu m$	$z = 6.00\,\mu m$	$z = 7.00\,\mu m$	$z = 8.00\,\mu m$
0 V	0.000	0.000	0.000	000.0	0.000	0.000	0.000	0.000	0.000
1 V	0.106	0.090	0.065	0.084	0.102	0.108	0.061	0.078	0.104
2 V	0.185	0.159	0.117	0.148	0.179	0.189	0.112	0.138	0.183
3 V	0.257	0.223	0.168	0.209	0.250	0.263	0.161	0.195	0.255

Table III: Phase shift values calculated for a **deep** etch $10.0\,\mu m$-long device at different z-cuts. The waveguide is excited from the end, so $z = 0.00\,\mu m$ is the last plane of propagation.

	$\Delta\Phi_{\frac{\pi}{mm}}(V_{bias})$								
V_{bias}	$z = 0.00\,\mu m$	$z = 1.00\,\mu m$	$z = 2.00\,\mu m$	$z = 3.00\,\mu m$	$z = 4.00\,\mu m$	$z = 5.00\,\mu m$	$z = 6.00\,\mu m$	$z = 7.00\,\mu m$	$z = 8.00\,\mu m$
0 V	0.000	0.000	0.000	0.000	0.000	0.000	0.000	0.000	0.000
1 V	0.068	0.043	0.071	0.049	0.067	0.055	0.064	0.040	0.034
2 V	0.120	0.078	0.127	0.089	0.119	0.098	0.114	0.072	0.061
3 V	0.168	0.112	0.178	0.126	0.168	0.139	0.160	0.103	0.087

Table IV: Phase shift values calculated for a **shallow** etch $10.0\,\mu m$-long device at different z-cuts. The waveguide is excited from the end, so $z = 0.00\,\mu m$ is the last plane of propagation.

[5] G. T. Reed, G. Mashanovich, F. Y. Gardes and D. J. Thomson, *Silicon optical modulators*, *Nature Photonics*, vol. 4, pp. 518-526, 2010.

[6] S. Seif El Nasr-Storey, *Radiation-hard Optoelectronics for LHC detector upgrades*, PhD Thesis, 2016.

[7] O. Powell, *Single-mode condition for silicon rib waveguides*, *Journal of Lightwave Technologies*, vol. 20, pp. 18511855, 2002.

[8] Synopsys^{TM}, *Sentaurus^{TM} Device Electromagnetic Wave Solver User Guide*, Version L-2016.03, 2016.

[9] Synopsys^{TM}, *Sentaurus^{TM} Device User Guide*, Version L-2016.03, 2016.

[10] G. T. Reed, A. P. Knights, *Silicon Photonics: An Introdution*, John Wiley & Sons Ltd, pp.63-65, 2004.

[11] Synopsys^{TM}, *TCAD software*, https://www.synopsys.com/silicon/tcad.html.

[12] Phoenix^{TM}, *OptoDesigner^{TM} software*, http://www.phoenixbv.com/.